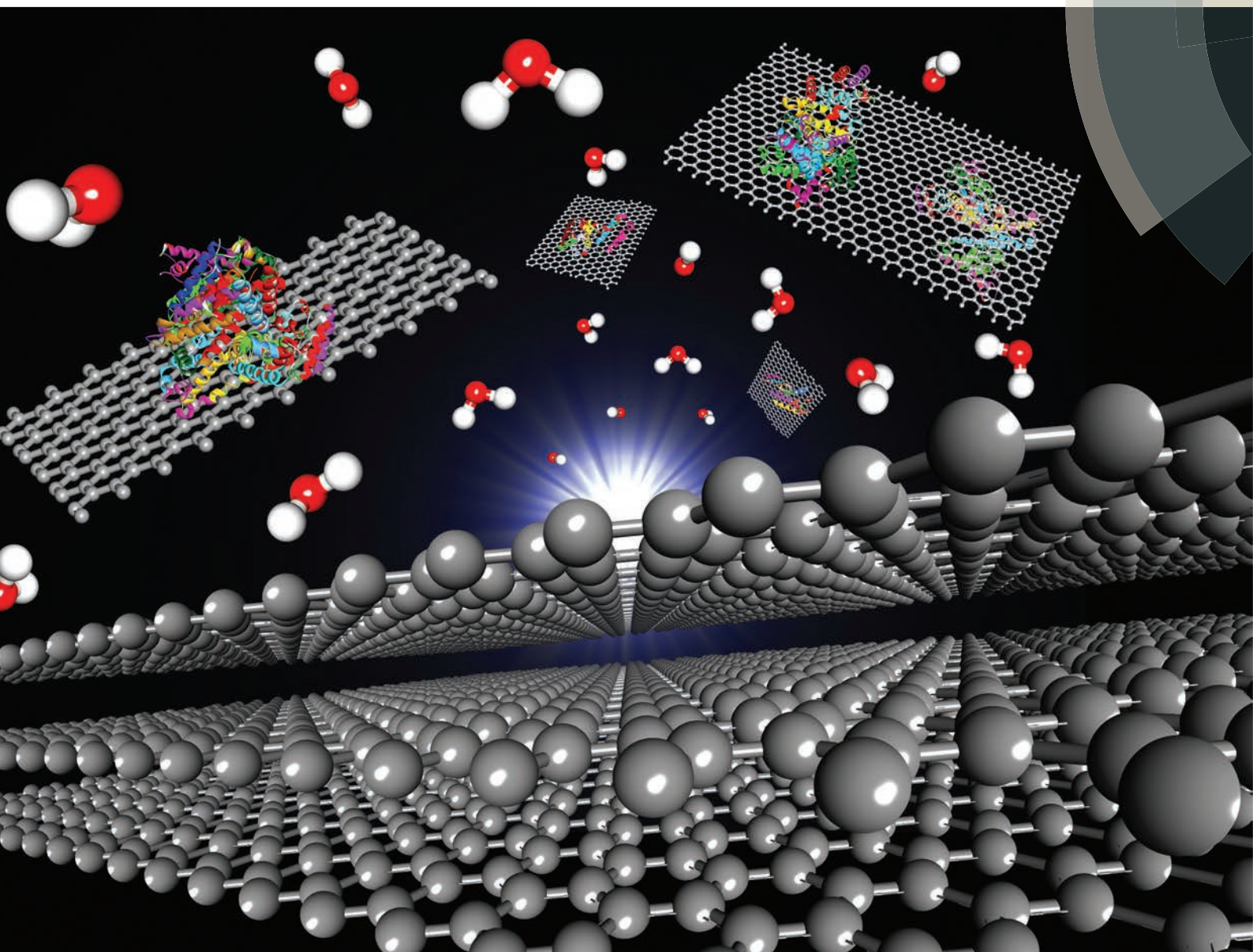


Nanoscale

www.rsc.org/nanoscale



ISSN 2040-3364



ROYAL SOCIETY
OF CHEMISTRY

COMMUNICATION

Mehdi Estili, Ali Khademhosseini *et al.*

Facile and green production of aqueous graphene dispersions for biomedical applications





Cite this: *Nanoscale*, 2015, 7, 6436

Received 23rd December 2014,

Accepted 27th January 2015

DOI: 10.1039/c4nr07569b

www.rsc.org/nanoscale

Facile and green production of aqueous graphene dispersions for biomedical applications†

Samad Ahadian,^a Mehdi Estili,^{*b} Velappa Jayaraman Surya,^c Javier Ramón-Azcón,^a Xiaobin Liang,^a Hitoshi Shiku,^d Murugan Ramalingam,^{a,e,f} Tomokazu Matsue,^{a,d} Yoshio Sakka,^g Hojae Bae,^h Ken Nakajima,^a Yoshiyuki Kawazoe^{c,m} and Ali Khademhosseini^{*a,h,i,j,k,l}

We proposed a facile, low cost, and green approach to produce stable aqueous graphene dispersions from graphite by sonication in aqueous bovine serum albumin (BSA) solution for biomedical applications. The production of high-quality graphene was confirmed using microscopy images, Raman spectroscopy, UV-vis spectroscopy, and XPS. In addition, *ab initio* calculations revealed molecular interactions between graphene and BSA. The processability of aqueous graphene dispersions was demonstrated by fabricating conductive and mechanically robust hydrogel-graphene materials.

Graphene consists of sp²-hybridized carbon atoms that form a one-atom-thick, two-dimensional honeycomb-like hexagonal structure. Graphene was discovered in 2004¹ and since then has found many applications in nanoscience and nanotechnology.² In particular, graphene has emerged as a functional material in biomedicine (*e.g.* gene and drug delivery,³ photothermal therapy,⁴ biosensing,⁵ bioimaging and monitoring,⁶ cell-based studies,⁷ and as tissue engineering scaffolds⁸) because of its unique electronic, mechanical, chemical, and optical properties.

Because most biological media are aqueous,⁹ the preparation of stable and processable aqueous graphene dispersions is essential for using graphene in biomedical applications. However, pristine graphene nanosheets are unstable in aqueous media and tend to aggregate because of van der Waals interactions.¹⁰ A commonly used approach to make aqueous graphene dispersions is by liquid-exfoliation of graphite in water using a sonication procedure.¹¹ However, some exogenous materials (*e.g.* organic solvents,¹² ionic liquids,¹³ and surfactants¹⁴) and sometimes additional experimental steps (*e.g.* using electrochemical potentials¹⁵) are required to obtain stable graphene dispersions in water. This approach has been successful in producing high-quality graphene with minimized oxide defects. However, toxicity and lack of biocompatibility of the used materials or techniques have restricted the safe use of produced graphene in biomedical applications. Another approach for preparing aqueous graphene dispersions involves reducing (thermally or chemically) water-dispersible graphene oxide.¹⁶ However, the production and reduction of graphene oxide require the use of toxic or explosive chemicals, such as sulfuric acid (H₂SO₄), hydrazine, and potassium permanganate (KMnO₄), or long and complicated processes.¹⁷ In addition, the crystalline structure and electronic properties of the synthesized graphene are not well preserved because of the formation of defects and the remaining chemical groups in graphene.¹⁸ Therefore, the preparation of stable and processable aqueous graphene dispersions using a facile and green approach for biomedical applications remains a challenge.

^aWPI-Advanced Institute for Materials Research, Tohoku University, Sendai 980-8577, Japan

^bInternational Center for Young Scientists (ICYS), National Institute for Materials Science (NIMS), Tsukuba 305-0047, Japan. E-mail: estili.mehdi@nims.go.jp; Fax: +81 29 859 2200

^cNew Industry Creation Hatchery Center, Tohoku University, Sendai 980-8579, Japan

^dGraduate School of Environmental Studies, Tohoku University, Sendai 980-8579, Japan

^eCentre for Stem Cell Research, A unit of the Institute for Stem Cell Biology and Regenerative Medicine, Christian Medical College Campus, Vellore 632002, India

^fInstitut National de la Santé Et de la Recherche Médicale U977, Faculté de Chirurgie Dentaire, Université de Strasbourg, Strasbourg 67085, France

^gMaterials Processing Unit, NIMS, Tsukuba 305-0047, Japan

^hCollege of Animal Bioscience and Technology, Department of Bioindustrial Technologies, Konkuk University, Hwayang-dong, Kwangjin-gu, Seoul 143-701, Republic of Korea

ⁱDepartment of Medicine, Biomaterials Innovation Research Center, Brigham and Women's Hospital, Harvard Medical School, Cambridge, Massachusetts 02139, USA. E-mail: alikh@rics.bwh.harvard.edu; Fax: +1 617 768 8477

^jHarvard-MIT Division of Health Sciences and Technology, Massachusetts Institute of Technology, Cambridge, Massachusetts 02139, USA

^kWyss Institute for Biologically Inspired Engineering, Harvard University, Boston, Massachusetts 02115, USA

^lDepartment of Physics, Faculty of Science, King Abdulaziz University, Jeddah 21569, Saudi Arabia

^mInstitute of Thermophysics, Siberian Branch of Russian Academy of Sciences, Novosibirsk 630090, Russia

† Electronic supplementary information (ESI) available: Fig. S1–S5, Tables S1 and S2, and the Experimental section. See DOI: 10.1039/c4nr07569b

Here, we propose a facile, green, and inexpensive approach for preparing stable aqueous graphene dispersions, which involves the exfoliation and fragmentation of graphite into graphene through sonication in bovine serum albumin (BSA) aqueous solution. Graphite is a ubiquitous and natural material, and BSA is a natural protein derived from cow. In this study, we synthesized and characterized graphene; we also performed first-principles calculations to understand the molecular interactions between graphene and BSA during the graphene production. Furthermore, we demonstrated the functionality of these aqueous graphene dispersions by fabricating conductive and mechanically robust hybrid hydrogel-graphene materials.

Graphite was exfoliated and broken down to graphene under sonication conditions in an aqueous BSA solution (Fig. 1A). We sonicated the graphite with a power of 15 W cm^{-2} at $25 \text{ }^\circ\text{C}$ in which the structural properties of BSA remain unchanged.¹⁹ The acoustic cavitation of ultrasonic waves led to the formation, development, and collapse of bubbles in water, which induced shock waves on the graphite that resulted in its exfoliation and fragmentation. Subsequently, few-layered graphene nanosheets interacted with the BSA molecules, which

stabilized them in water. The large surface area of hydrophobic graphene enabled effective adsorption of the hydrophobic segments of BSA, whereas the hydrophilic segments of BSA interacted with water. The concentration of graphene dispersion could be adjusted by changing the concentration of BSA in the medium (Fig. 1B). Notably, graphite could not be dispersed in water in the absence of BSA, which was used as a negative control in our experiments. The aqueous graphene dispersions were highly stable, and no aggregation or precipitation of graphene occurred even after storage under ambient conditions for a couple of months. It is believed that BSA stabilized the graphene through non-covalent bonding, which has certain advantages over stabilization through covalent bonding, such as minimal alterations in the structure and intrinsic properties of graphene.²⁰ Transmission electron microscopy (TEM) images of the graphene (Fig. 1C) revealed the successful isolation of graphene nanosheets. According to the scanning electron microscopy (SEM) images (Fig. 1D), graphene was the major constituent of aqueous dispersion and a negligible amount of graphite was observed. In addition, the images showed that most graphene sheets had a maximum lateral dimension from tens of nm to a few μm . As shown in Fig. 1E,

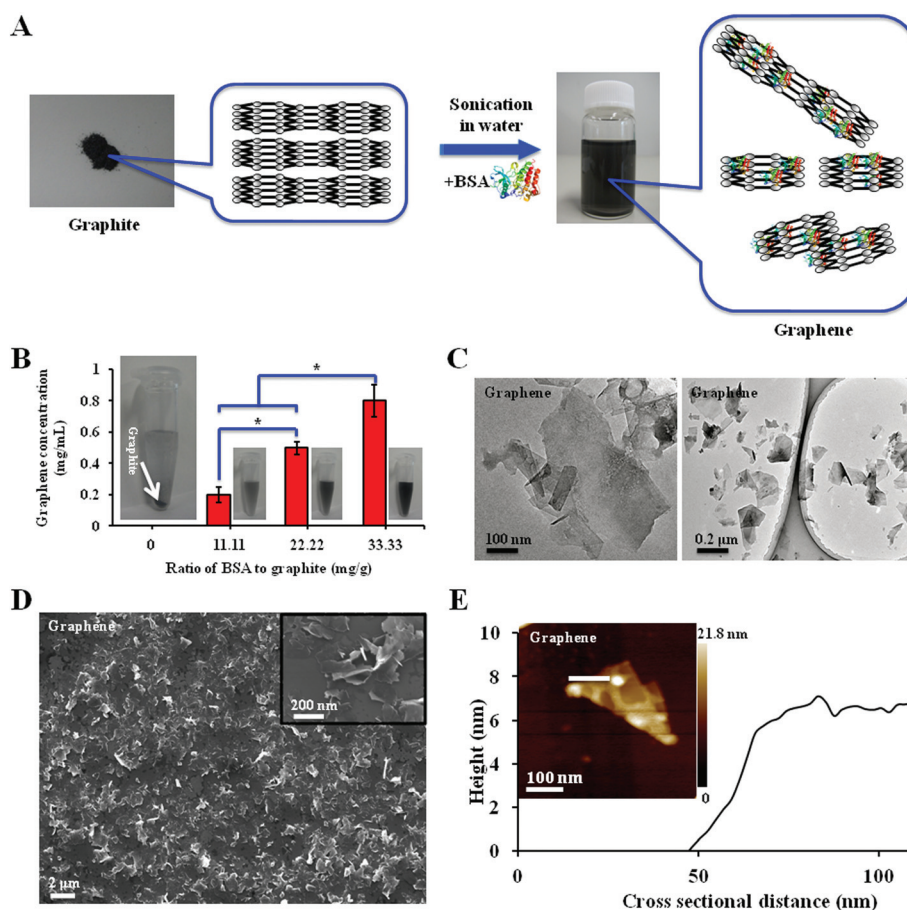


Fig. 1 Synthesis, structural and morphological properties of BSA-solution stabilized few-layered graphene. (A) Pictures and schematic representation of the fabrication of aqueous graphene dispersion from graphite. (B) Different concentrations of graphene dispersion as a function of BSA concentration in the medium ($*p < 0.05$). Representative pictures are shown to the right of the corresponding bars. (C) TEM images of graphene. (D) SEM images of graphene. (E) AFM image and corresponding height profile of graphene.

we used atomic force microscopy (AFM) to analyze the thickness of the graphene nanosheets after stabilization with BSA. The height-profile images of the graphene sheets revealed that they had a thickness of 6.7 ± 4.6 nm, suggesting the presence of single-layered to few-layered graphene sheets in the aqueous dispersion. Note that the relatively high thickness of fabricated graphene is because of the adsorbed BSA on its surface.

The Raman spectrum of the graphite (Fig. 2A) clearly showed the D, G, and 2D bands at ~ 1328 , ~ 1578 , and ~ 2731 cm^{-1} , respectively, which are the characteristic bands of pristine graphite.²¹ For synthesized graphene (Fig. 2A), the D, G, and 2D bands were located at ~ 1349 , ~ 1568 , and ~ 2700 cm^{-1} , respectively, showing high-quality graphene. The ratio of the D to G band intensities for graphite, 0.02,

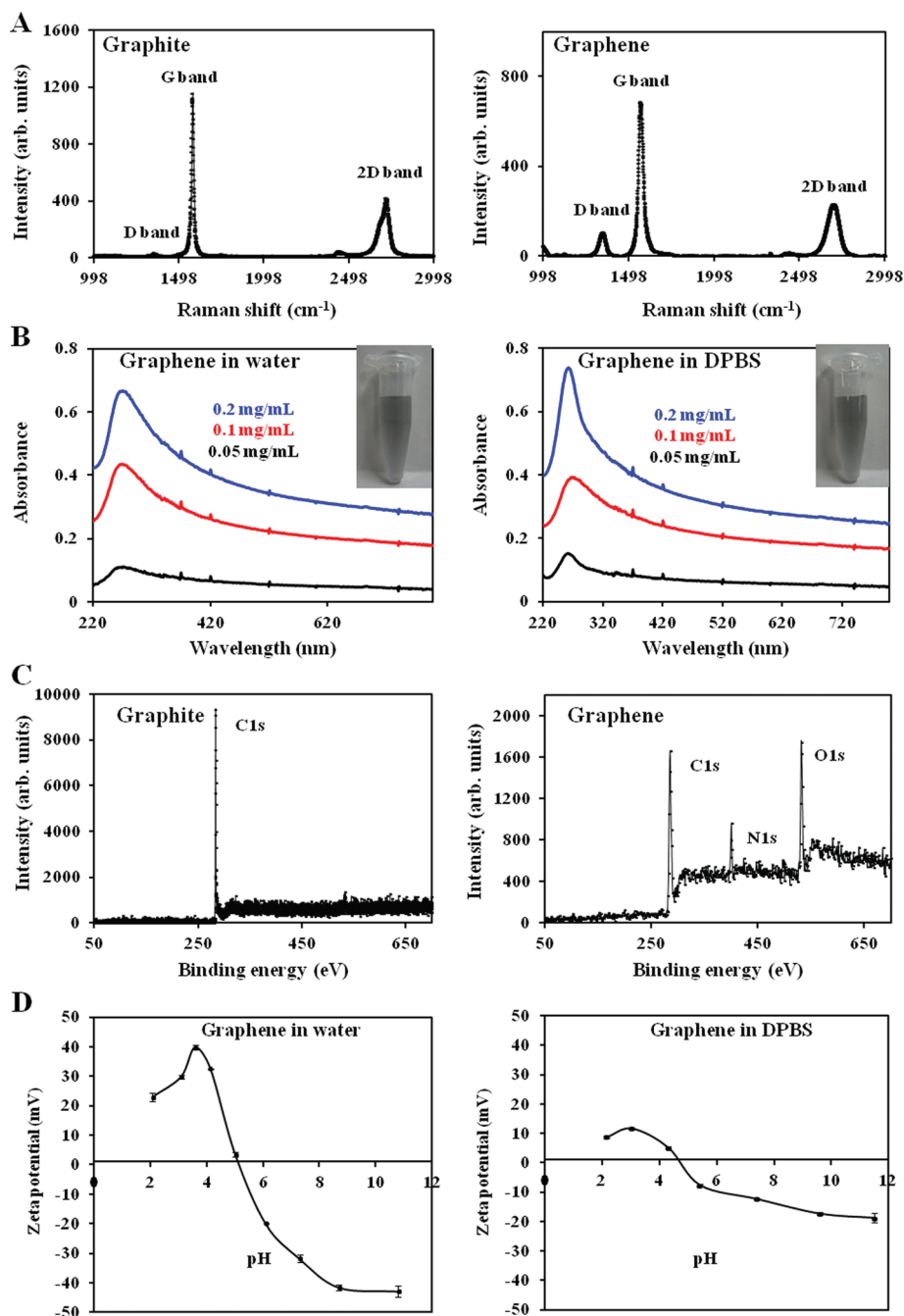


Fig. 2 Characteristics of graphene. (A) Raman spectra for graphite and graphene. The D, G, and 2D bands were detectable for both graphite and graphene. (B) UV-vis spectra for graphene in water and graphene in DPBS at three different concentrations (*i.e.* 0.05, 0.1, and 0.2 mg mL^{-1}). Pictures of 0.2 mg mL^{-1} graphene in water and 0.2 mg mL^{-1} graphene in DPBS are shown at the top right of the plots. (C) C 1s, N 1s, and O 1s XPS analyses of graphite and graphene. (D) Zeta potentials for graphene in water and graphene in DPBS at different pH values.

increased to 0.15 for graphene, most likely because of an increase in the number of aromatic domains in graphene compared with graphite.²² Interestingly, the symmetry of the 2D band was greater for graphene than for graphite. The lack of 2D-band symmetry in graphite is due to the perfect stacking order of the graphene layers in graphite. The evolution of symmetry in graphene indicates the disruption of the graphite stacking order²³ as a result of graphene production.

We further confirmed the presence of graphene in the aqueous dispersion using UV-vis spectroscopy. As shown in Fig. 2B, the largest absorbance peak in the UV-vis spectra was observed at ~ 269 nm for different concentrations of graphene in aqueous medium (*i.e.* 0.05, 0.1, and 0.2 mg mL⁻¹), which is a characteristic of graphene.²⁴ As shown in Fig. 2C and Fig. S1,† the N 1s signal was clearly observed in the XPS scan survey for graphene compared with that for graphite, indicating that BSA was adsorbed on graphene. The atomic concentrations of N 1s for graphite and graphene were 0 and 13.8%, respectively. Detailed XPS analyses of graphite and graphene are given in Table S1;† these analyses reveal different functional groups on graphene because of the BSA adsorbed on its surface.

We evaluated the electrostatic colloidal stability of graphene in both water and Dulbecco's phosphate-buffered saline (DPBS) solution (a water-based saline solution) by performing zeta potential measurements under various pH conditions. In both water and DPBS, the graphene was positively and negatively charged at pH values below and above ~ 5 , respectively. Therefore, pH ~ 5 is considered as the isoelectric point of graphene in water and in DPBS, in which graphene has the lowest stability in the medium. Such a behavior is similar to that of BSA in water,²⁴ suggesting that the colloidal stability of graphene is due to the electrostatic repulsion of charged BSA molecules on graphene. A high zeta potential of $\sim +40$ mV was obtained at pH 3.6 for the graphene dispersion in water, indicating excellent colloidal stability of the dispersion. A decrease in the zeta potential upon decreasing the pH from 3.6 occurs due to an increase in the ionic strength of water, which impaired the stability of graphene in water. In DPBS solution, however, the zeta potential values were lower than those measured in water (Fig. 2D), which was attributed to the higher ionic strength of DPBS relative to that of water. The latter was confirmed by measuring the ionic conductivity of graphene in water and DPBS solutions at pH ~ 3.6 (0.513 and 1.105 S m⁻¹, respectively). Despite the low zeta potential values observed for graphene in DPBS (*e.g.* -12 mV at pH ~ 3), no immediate aggregation of graphene in DPBS was observed (Fig. 2B, inset), and the corresponding UV-vis spectrum was almost comparable to that of graphene in water (Fig. 2B).

We drop-casted graphene dispersion (0.2 mg mL⁻¹) on a glass slide and allowed for water evaporation to make graphene substrates. About 80% of the glass slides were covered by graphene. As reported in our previous study,⁸ this amount of graphene significantly increases the surface roughness of glass slides. The Young's modulus of graphene substrates was ~ 4 GPa, while that of glass slides was ~ 70 GPa.⁸

C2C12 myoblasts cultured on graphene substrates exhibited high cell viability and proliferation compared to those cultured on conventional Petri dishes, indicating that the synthesized graphene possessed biocompatibility suitable for biomedical applications (Fig. S2†). The viability of muscle cells on graphene was greater than 98% during the 5 days of culture. The proliferation rate of cells on graphene and that of cells on Petri dish substrates were not statistically different except for 3 days after the muscle cell culture, when the cells proliferated faster on the graphene substrate than on the Petri dish. The proliferation rates were $258 \pm 7\%$ and $244 \pm 9\%$ for the C2C12 myoblasts proliferated on the graphene and control substrates, respectively, at day 3 of culture. The latter result is most likely due to the higher adhesion and spreading of muscle cells on graphene than on Petri dishes. It is well known that the adhesion of muscle cells is a prerequisite for effective cell proliferation and differentiation.²⁵ Duch *et al.* reported that well-dispersed and non-oxidized graphene had the least *in vivo* toxicity compared with graphene oxide and graphene agglomerates.²⁶ Girish *et al.* recently reported the biodegradation of graphene *in vivo*.²⁷ Furthermore, Li *et al.* demonstrated that coating graphene oxide with BSA significantly reduced its cytotoxicity with a substantial increase in its enzymatic biodegradability.²⁸ Taken together, we believe that our aqueous graphene dispersion may attract considerable attention in biomedicine, particularly for *in vivo* applications.

We performed density functional theory (DFT) calculations to determine the molecular interactions between graphene and BSA. The peptide sequence of BSA contains 290 hydrophobic (non-polar) and 293 hydrophilic (polar) amino acids that are randomly distributed within the BSA peptide chain.²⁹ Here, we hypothesized that only the hydrophobic amino acids of BSA interacted with graphene during the graphene production. There are eleven types of hydrophobic amino acids in a BSA molecule, namely alanine (Ala), cysteine (Cys), glycine (Gly), isoleucine (ILeu), leucine (Leu), methionine (Met), phenylalanine (Phe), proline (Pro), tryptophan (Tryp), tyrosine (Tyr), and valine (Val).²⁹ Ala, Gly, ILeu, Leu, and Val are aliphatic amino acids that have saturated hydrocarbons as side chains, except for Gly. Pro is an imino acid having both imino and carboxyl groups. Cys and Met are sulfur-containing amino acids. Phe, Tyr, and Tryp are aromatic amino acids.²⁹ The molecular interactions between graphene and these amino acids were studied using binding energy, charge transfer, and density of states (DOS) analyses, as described below.

The optimized structures of graphene with all underlying amino acids are shown in Fig. 3A and S3.† The rings of the aromatic amino acids were oriented parallel to the graphene surface. The calculated binding energies of the amino acid moieties with graphene are presented in Table S2.† All of the amino acids were physisorbed on graphene with an intermolecular distance (defined as the distance between the plane of the graphene and the closest atom of the amino acid to the graphene) in the range of 2.7–3.9 Å (Table S2†). These findings indicated that non-covalent interactions (van der Waals and electrostatic interactions) are primarily dominant among the

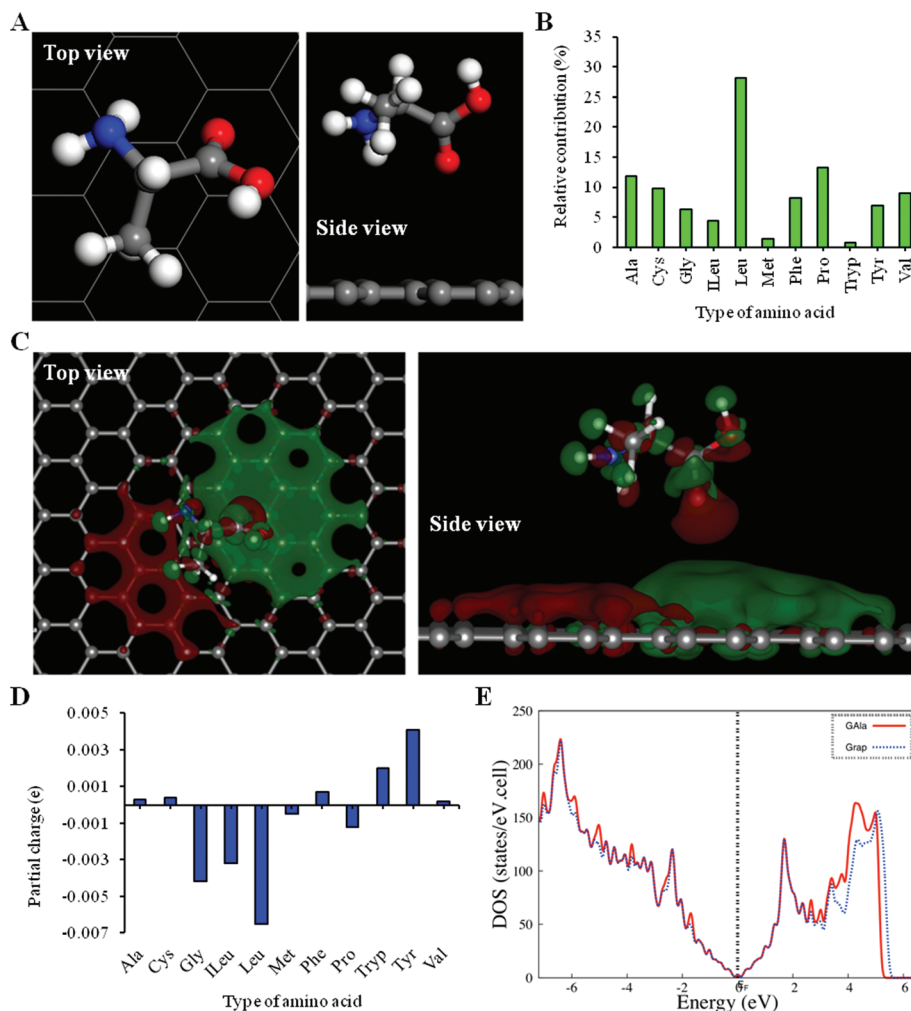


Fig. 3 DFT calculation results for elucidating the molecular interactions of graphene with BSA. (A) Optimized structure of graphene with Ala from top and side views. White, grey, blue, and red balls represent H, C, N, and O atoms, respectively. (B) Levels of contribution by individual amino acids of BSA to the stabilization of graphene in water. (C) Isosurface charge density plot of graphene with Ala from top and side views. White, grey, blue, and red balls represent H, C, N, and O atoms, respectively. (D) Partial charge on amino acids adsorbed on graphene. (E) Total DOS plots of graphene with Ala. Red and dashed blue lines show the DOS plots of the graphene–amino acid complex and of pristine graphene, respectively.

two entities, essentially due to X–H... π (X = C, O, and N) and π – π stacking interactions of aliphatic and aromatic amino acids with graphene, respectively. Although such interactions are weak, they are responsible for the stabilization of various biomolecules on graphene.³⁰ With regard to the aromatic amino acids, the trend of binding energies was in the order of Tryp > Tyr > Phe, which is consistent with a previous theoretical report.³¹ To determine the contribution of each amino acid to the peeling of graphene sheets from graphite, the binding energy values were multiplied by the number of corresponding amino acids present in BSA. The result shows the following trend: Leu > Pro > Ala > Cys > Val > Phe > Tyr > Gly > Ileu > Met > Tryp (Fig. 3B). The architectural aspects of BSA (e.g. protein structure or folding) may also affect the graphene exfoliation, which were not considered for the calculations because of limited computational capabilities of the DFT approach.

The charge density difference plots are shown in Fig. 3C and S4.† The values of partial charges on all amino acids are presented in Fig. 3D. The presence of electronegative atoms, such as O, N, and S in the aliphatic, imino, and sulfur-containing amino acids, respectively, was responsible for the withdrawal of electrons from the graphene, whereas the aromatic acids primarily interacted with graphene through aromatic rings lying parallel to the graphene sheet. Fig. 3E and S5† show the total DOS of the graphene–amino acid complexes plotted with reference to pristine graphene. There was no significant distortion at the Fermi level in any of the graphene–amino acid systems, indicating a non-covalent interaction between the graphene and the amino acids. The physisorption of all of the amino acids on the graphene introduced a Fermi level shift of ~3–78 meV to higher energy compared to that of pristine graphene. Overall, the DFT investigation demonstrated that the aliphatic side chains and aromatic rings in the hydro-

phobic amino acids of BSA were responsible for the non-covalent interaction of BSA with graphene that enabled the stabilization of graphene sheets in water. Therefore, it can be concluded that both hydrophobic and hydrophilic regions in BSA effectively interacted with graphene and water, respectively and have significant effects on producing a stable aqueous graphene dispersion. In general, other natural and biocompatible materials can also be used for the stabilization of graphene sheets obtained from exfoliated natural graphite in water for potential biomedical applications as long as they contain both active hydrophobic and hydrophilic regions in their structure. It seems that other proteins are good candidates to replace BSA in graphene production. In this regard, DFT calculations may reveal useful information on the nature of molecular interactions between graphene and proteins. In addition, it would be possible to understand which protein (both structurally and energetically) is the most suitable one for graphene production. The use of adsorbed proteins on graphene to

deliver biomolecules, such as genes and drugs, may also be a great avenue of research in the future.

To demonstrate the functionality of our synthesized graphene for biomedical applications, graphene was used as an efficient supplementary material to increase the conductivity and Young's modulus of hydrophilic hydrogels. For this purpose, pristine methacrylated gelatin (GelMA) and GelMA-graphene hydrogels were prepared. The methacrylation degree of GelMA hydrogels and their concentrations were $\sim 80\%$ and 10% (w/v), respectively. The DC conductivities of all of these materials are reported in Fig. 4A. The DC current conductance dramatically increased as graphene was added to the GelMA hydrogels. The impedance of hydrogels exhibited a similar trend (Fig. 4B). The higher electrical conductivities of the GelMA-graphene hydrogels compared with those of the pure GelMA gels were attributed to the extremely high electrical conductivity of graphene. Hydrogels have been used in various biomedical applications owing to their biocompatibility and

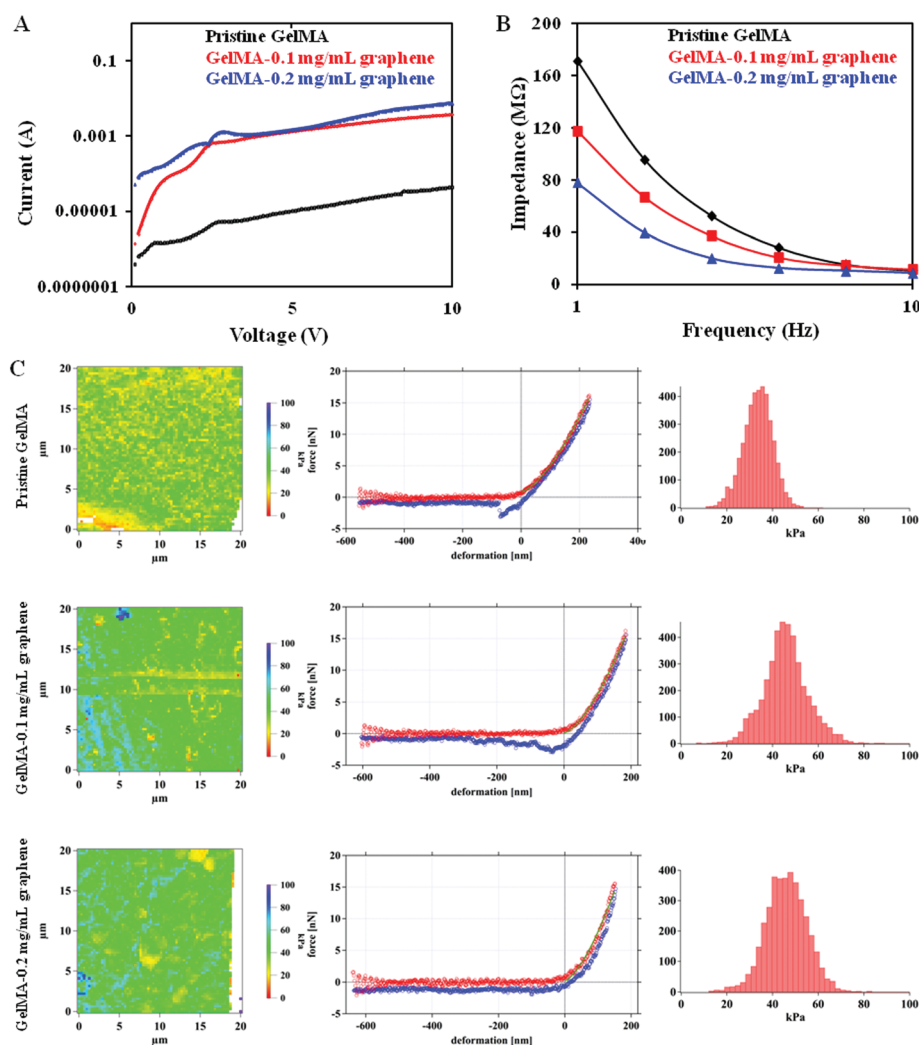


Fig. 4 Electrical and Young's modulus of pure GelMA (10% [w/v]) and GelMA-graphene gels loaded with 0.1 and 0.2 mg mL^{-1} graphene. (A) I - V curves for pure GelMA and GelMA gels containing graphene. (B) Impedance values of pure GelMA and hybrid hydrogels including 0.1 and 0.2 mg mL^{-1} graphene. The perturbation amplitude was set to be 25 mV. (C) Young's modulus map, force deformation curves, and Young's modulus distribution (left to right, respectively) measured by AFM for pure GelMA and for hybrid GelMA graphene hydrogels.

tunable physical and chemical properties.³² However, hydrogels generally have low electrical conductivity, which limits their efficiency in certain applications.³³ For example, electrically conductive hydrogels have a higher performance compared with hydrogels with low conductivity to regulate behaviors of electro-active cells, such as skeletal muscle, neural, and cardiac cells and fabricate their tissues constructs.³⁴ In particular, electrical stimulation would be more effective for cells encapsulated in such conductive hydrogels to fabricate functional and electrically-responsive tissues.³⁵ Taken together, graphene-hydrogel materials with enhanced electrical properties have the desired functionality for biomedical applications.

In this investigation, an AFM-based micromechanical mapping technique was employed to quantify the mechanical properties of GelMA-graphene hydrogels. The Young's modulus for 10% (w/v) pure GelMA was 33.5 ± 6.7 kPa (Fig. 4C). Because the GelMA was reinforced by graphene, the Young's moduli increased to 45.8 ± 9.9 and 46.1 ± 11.2 kPa for the GelMA-0.1 mg mL⁻¹ graphene and GelMA-0.2 mg mL⁻¹ graphene hydrogels, respectively. The mechanically strong graphene encapsulated in the GelMA hydrogels enhanced the Young's moduli of hybrid hydrogels. Different cellular behaviors, such as morphology and adhesion, are affected by the mechanical properties of hydrogels.³⁶ Therefore, tuning the mechanical properties of hydrogels is of great interest for cell-based studies. Particularly, Young's modulus of hydrogels is a key parameter taken into account to regulate stem cell behaviors and direct their differentiation and fate.³⁷ Hydrogels having tunable Young's modulus provide a simple, versatile, and controllable platform to study mechanobiology and differentiation of stem cells. In addition, hydrogels with tunable mechanical properties are desirable for other biomedical applications, such as materials for electronic-tissue interfaces³⁸ and as bioactuators.³⁹ In this regard, the use of water-dispersible graphene in hydrogels is a useful approach to provide the mechanically tunable gels with widespread applications in biomedicine.

In summary, we have proposed a facile and green approach for preparing stable aqueous graphene dispersions suitable for various biomedical applications. This approach, which is simply the exfoliation and fragmentation of graphite powder in an aqueous BSA solution, enabled us to produce stable aqueous graphene dispersions at low cost and without the need for hazardous chemicals or tedious experimental procedures. In addition, we demonstrated the processability of such aqueous graphene dispersions by fabricating GelMA hydrogel-graphene materials. The fabricated hybrids exhibited tunable stiffness and considerably higher electrical conductivity than did pure GelMA hydrogels.

Acknowledgements

S.A. acknowledges Professor Mingwei Chen and Dr Ling Zhang from Tohoku University, Japan, for providing the UV-vis

spectrophotometer. S.A. acknowledges the discussion with Dr Mohammad Khazaei from NIMS, Japan, regarding the first-principles calculations. V.J.S. and Y.K. would like to thank the staff of the Center for Computational Materials Science of the Institute for Materials Research, Tohoku University, for their continuous support of the SR16000 supercomputing facilities. Y.K. is thankful to the Russian Megagrant Project No. 14.B25.31.0030 "New energy technologies and energy carriers" for supporting the present research. This work was supported by the ICYS grant from NIMS, Japan, to M.E. and by the World Premier International Research Center Initiative (WPI), MEXT, Japan.

Notes and references

- 1 K. S. Novoselov, A. K. Geim, S. V. Morozov, D. Jiang, Y. Zhang, S. V. Dubonos, I. V. Grigorieva and A. A. Firsov, *Science*, 2004, **306**, 666–669.
- 2 K. S. Novoselov, V. I. Falko, L. Colombo, P. R. Gellert, M. G. Schwab and K. Kim, *Nature*, 2012, **490**, 192–200.
- 3 Z. Liu, J. T. Robinson, S. M. Tabakman, K. Yang and H. Dai, *Mater. Today*, 2011, **14**, 316–323.
- 4 O. Akhavan and E. Ghaderi, *Small*, 2013, **9**, 3593–3601.
- 5 J. S. Lee, H.-A. Joung, M.-G. Kim and C. B. Park, *ACS Nano*, 2012, **6**, 2978–2983.
- 6 T. Cohen-Karni, Q. Qing, Q. Li, Y. Fang and C. M. Lieber, *Nano Lett.*, 2010, **10**, 1098–1102.
- 7 W. Li, J. Wang, J. Ren and X. Qu, *Angew. Chem., Int. Ed.*, 2013, **52**, 6726–6730.
- 8 S. Ahadian, J. Ramón-Azcón, H. Chang, X. Liang, H. Kaji, H. Shiku, K. Nakajima, M. Ramalingam, H. Wu, T. Matsue and A. Khademhosseini, *RSC Adv.*, 2014, **4**, 9534–9541.
- 9 C. Cha, S. R. Shin, N. Annabi, M. R. Dokmeci and A. Khademhosseini, *ACS Nano*, 2013, **7**, 2891–2897.
- 10 D. Li, M. B. Muller, S. Gilje, R. B. Kaner and G. G. Wallace, *Nat. Nanotechnol.*, 2008, **3**, 101–105.
- 11 X. Cui, C. Zhang, R. Hao and Y. Hou, *Nanoscale*, 2011, **3**, 2118–2126.
- 12 E. Ou, Y. Xie, C. Peng, Y. Song, H. Peng, Y. Xiong and W. Xu, *RSC Adv.*, 2013, **3**, 9490–9499.
- 13 J. Lu, J.-x. Yang, J. Wang, A. Lim, S. Wang and K. P. Loh, *ACS Nano*, 2009, **3**, 2367–2375.
- 14 S. Haar, A. Ciesielski, J. Clough, H. Yang, R. Mazzaro, F. Richard, S. Conti, N. Merstorf, M. Cecchini, V. Morandi, C. Casiraghi and P. Samori, *Small*, 2014, DOI: 10.1002/smll.201402745.
- 15 N. Liu, F. Luo, H. Wu, Y. Liu, C. Zhang and J. Chen, *Adv. Funct. Mater.*, 2008, **18**, 1518–1525.
- 16 H. Feng, R. Cheng, X. Zhao, X. Duan and J. Li, *Nat. Commun.*, 2013, **4**, 1539.
- 17 W. S. Hummers and R. E. Offeman, *J. Am. Chem. Soc.*, 1958, **80**, 1339–1339.
- 18 Q. He, S. Wu, S. Gao, X. Cao, Z. Yin, H. Li, P. Chen and H. Zhang, *ACS Nano*, 2011, **5**, 5038–5044.
- 19 İ. Gülseren, D. Güzey, B. D. Bruce and J. Weiss, *Ultrason. Sonochem.*, 2007, **14**, 173–183.

- 20 T. S. Sreeprasad and V. Berry, *Small*, 2013, **9**, 341–350.
- 21 F. Tuinstra and J. L. Koenig, *J. Chem. Phys.*, 1970, **53**, 1126–1130.
- 22 S. Stankovich, D. A. Dikin, R. D. Piner, K. A. Kohlhaas, A. Kleinhammes, Y. Jia, Y. Wu, S. T. Nguyen and R. S. Ruoff, *Carbon*, 2007, **45**, 1558–1565.
- 23 N. Xiao, X. Dong, L. Song, D. Liu, Y. Tay, S. Wu, L.-J. Li, Y. Zhao, T. Yu, H. Zhang, W. Huang, H. H. Hng, P. M. Ajayan and Q. Yan, *ACS Nano*, 2011, **5**, 2749–2755.
- 24 J. Liu, S. Fu, B. Yuan, Y. Li and Z. Deng, *J. Am. Chem. Soc.*, 2010, **132**, 7279–7281.
- 25 S. H. Ku and C. B. Park, *Biomaterials*, 2013, **34**, 2017–2023.
- 26 M. C. Duch, G. R. S. Budinger, Y. T. Liang, S. Soberanes, D. Urich, S. E. Chiarella, L. A. Campochiaro, A. Gonzalez, N. S. Chandel, M. C. Hersam and G. M. Mutlu, *Nano Lett.*, 2011, **11**, 5201–5207.
- 27 C. M. Girish, A. Sasidharan, G. S. Gowd, S. Nair and M. Koyakutty, *Adv. Healthcare Mater.*, 2013, **2**, 1489–1500.
- 28 Y. Li, L. Feng, X. Shi, X. Wang, Y. Yang, K. Yang, T. Liu, G. Yang and Z. Liu, *Small*, 2014, **10**, 1544–1554.
- 29 P. F. Spahr and J. T. Edsall, *J. Biol. Chem.*, 1964, **239**, 850–854.
- 30 H. Vovusha, S. Sanyal and B. Sanyal, *J. Phys. Chem. Lett.*, 2013, **4**, 3710–3718.
- 31 C. Rajesh, C. Majumder, H. Mizuseki and Y. Kawazoe, *J. Chem. Phys.*, 2009, **130**, 124911.
- 32 N. Annabi, A. Tamayol, J. A. Uquillas, M. Akbari, L. E. Bertassoni, C. Cha, G. Camci-Unal, M. R. Dokmeci, N. A. Peppas and A. Khademhosseini, *Adv. Mater.*, 2014, **26**, 85–124.
- 33 T. Dvir, B. P. Timko, M. D. Brigham, S. R. Naik, S. S. Karajanagi, O. Levy, H. Jin, K. K. Parker, R. Langer and D. S. Kohane, *Nat. Nanotechnol.*, 2011, **6**, 720–725.
- 34 S. Ahadian, J. Ramón-Azcón, S. Ostrovidov, G. Camci-Unal, H. Kaji, K. Ino, H. Shiku, A. Khademhosseini and T. Matsue, *Biomed. Microdevices*, 2013, **15**, 109–115.
- 35 S. Ahadian, S. Ostrovidov, V. Hosseini, H. Kaji, M. Ramalingam, H. Bae and A. Khademhosseini, *Organogenesis*, 2013, **9**, 87–92.
- 36 S. Ahadian, J. Ramón-Azcón, M. Estili, X. Liang, S. Ostrovidov, H. Shiku, M. Ramalingam, K. Nakajima, Y. Sakka, H. Bae, T. Matsue and A. Khademhosseini, *Sci. Rep.*, 2014, **4**, 4271.
- 37 Y. Sun and J. Fu, *Integr. Biol.*, 2013, **5**, 450–457.
- 38 L. Yang, Y. Li and Y. Fang, *Adv. Mater.*, 2013, **25**, 3881–3887.
- 39 S. R. Shin, S. M. Jung, M. Zalabany, K. Kim, P. Zorlutuna, S. B. Kim, M. Nikkhah, M. Khabiry, M. Azize, J. Kong, K.-T. Wan, T. Palacios, M. R. Dokmeci, H. Bae, X. Tang and A. Khademhosseini, *ACS Nano*, 2013, **7**, 2369–2380.